Homeostatic regulation of axonal Kv1.1 channels accounts for both synaptic and intrinsic modifications in the hippocampal CA3 circuit

Mickaël Zbili, Sylvain Rama, Maria-José Benitez, Laure Fronzaroli-Molinieres, Andrzej Bialowas, Norah Boumedine-Guignon, Juan José Garrido, Dominique Debanne

Proceedings of the National Academy of Sciences

Homeostatic regulation of axonal Kv1.1 channels accounts for both synaptic and intrinsic modifications in the hippocampal CA3 circuit

Mickael Zbili[1], Sylvain Rama[1], Maria-José Benitez[2], Laure Fronzaroli-Molinieres[1], Andrzej Bialowas[1], Norah Boumedine-Guignon[1], Juan José Garrido[2], and Dominique Debanne[1]

[1]UNIS, UMR_S 1072, INSERM, Aix-Marseille Université, 13015 Marseille, France

[2]Instituto Cajal, Consejo Superior de Investigaciones Cientificas (CSIC), Madrid 28002, Spain

Abstract:

Homeostatic plasticity of intrinsic excitability goes hand in hand with homeostatic plasticity of synaptic transmission. However, the mechanisms linking the two forms of homeostatic regulation have not been identified so far. Using electrophysiological, imaging, and immunohistochemical techniques, we show here that blockade of excitatory synaptic receptors for 2 to 3 d induces an up-regulation of both synaptic transmission at CA3–CA3 connections and intrinsic excitability of CA3 pyramidal neurons. Intrinsic plasticity was found to be mediated by a reduction of Kv1.1 channel density at the axon initial segment. In activity-deprived circuits, CA3–CA3 synapses were found to express a high release probability, an insensitivity to dendrotoxin, and a lack of depolarization-induced presynaptic facilitation, indicating a reduction in presynaptic Kv1.1 function. Further support for the down-regulation of axonal Kv1.1 channels in activity-deprived neurons was the broadening of action potentials measured in the axon. We conclude that regulation of the axonal Kv1.1 channel constitutes a major mechanism linking intrinsic excitability and synaptic strength that accounts for the functional synergy existing between homeostatic regulation of intrinsic excitability and synaptic transmission.

Introduction

Chronic modulation of activity regimes in neuronal circuits induces homeostatic plasticity. This implicates a regulation of both intrinsic excitability (homeostatic plasticity of intrinsic excitability) and synaptic transmission (homeostatic plasticity of synaptic transmission) to maintain network activity within physiological bounds (1). In most cases, these two forms of homeostatic plasticity act synergistically but involve different molecular actors. Homeostatic intrinsic plasticity is associated with the regulation of voltage-gated ion channels (2–9), while homeostatic synaptic plasticity involves the regulation of postsynaptic receptors to neurotransmitters (10–17) or the regulation of the readily releasable pool of synaptic vesicles (18–20). However, the function of voltage-gated ion channels is not limited to the control of intrinsic excitability. Several studies point to the role of axonal voltage-gated channels in shaping presynaptic action potential (AP) waveform and subsequently controlling neurotransmitter release and synaptic transmission (21–35). Moreover, some studies describe homeostatic plasticity of the AP waveform via voltage-gated channel regulation (36–38), while other studies report an absence of this phenomenon (39). Kv1.1 channels are responsible for the fast-activating, slow-inactivating D-type current (ID) in CA3 neurons. This current has been shown to create a delay in the onset of the first AP and to determine intrinsic excitability in various neuronal types, including CA1 and CA3 pyramidal neurons of the hippocampus (3, 40), L5 pyramidal neurons of the cortex (26, 34), and L2/3 fast-spiking interneurons of the somatosensory cortex (41, 42). Furthermore, Kv1.1 channels have been shown to control axonal AP width and subsequently presynaptic calcium entry and neurotransmitter release. In fact, pharmacological blockade of Kv1.1 channels broadens presynaptic APs and increases synaptic transmission at neocortical and hippocampal glutamatergic synapses and at cerebellar GABAergic synapses (21, 22, 26, 30, 32, 41, 43, 44). Moreover, Kv1.1 channels have been shown to be responsible for the phenomenon of depolarization-induced analog digital facilitation of synaptic transmission (d-ADF). In fact, at CA3–CA3 and L5–L5 synapses, a somatic subthreshold depolarization of the presynaptic cell leads to inactivation of axonal Kv1.1 channels, inducing the broadening of the presynaptic AP, an increase in spike-evoked calcium entry, and a facilitation of presynaptic glutamate release (26, 31, 33, 34, 45, 46). Therefore, Kv1.1 channels control both intrinsic excitability and glutamate release in CA3 pyramidal neurons. Kv1.1 channels have been shown to be involved in homeostatic regulation of neuronal excitability. Chronic activity enhancement by kainate application leads to an increase in ID current and a decrease in excitability in dentate gyrus granule cells (47). Conversely, chronic sensory deprivation leads to Kv1.1 channel down-regulation and enhancement of excitability in the avian cochlear nucleus (48). In this study, we examined whether the increase in synaptic transmission could also be due to Kv1.1 channel down-regulation, which would possibly explain the observed synergy between homeostatic plasticity of excitability and synaptic transmission. We show here that chronic activity deprivation induced with an antagonist of ionotropic glutamate receptors (kynurenate) in hippocampal organotypic cultures provokes both an increase in CA3 pyramidal cells excitability and an enhancement of synaptic transmission at monosynaptically connected CA3 neurons. Deprived cultures display a decrease in Kv1.1 channel staining in the axon initial segment. Bath application of dendrotoxin-K (DTX-K), a selective blocker of Kv1.1 channels, leads to a larger excitability increase in control cultures than in deprived cultures. Focal puffing of DTX-K on the axon increases excitability in control but not in deprived cultures, showing that homeostatic plasticity of excitability in deprived cultures is partly due to the down-regulation of axonal Kv1.1 channels. In addition, we found that axonal Kv1.1 downregulation in deprived cultures is responsible for a spike broadening in CA3 neurons, leading to elevated release probability at CA3–CA3 synapses. Consistent with these observations, d-ADF, a Kv1.1-dependent form of synaptic facilitation, is present in control cultures but not in deprived cultures. Altogether, these results show that chronic activity

blockade of the hippocampal CA3 circuit induces the down-regulation of axonal Kv1.1 channels leading to a homeostatic increase in both excitability and presynaptic release probability.

Results

Increased Excitability and Synaptic Transmission in Activity-Deprived CA3 Circuits.

To determine the effect of chronic activity deprivation on the CA3 hippocampal network, we blocked excitatory synaptic transmission in hippocampal organotypic cultures (8 to 12 d in vitro [DIV]) with kynurenate (2 mM) for 2 to 3 d. We found an increase in CA3 pyramidal cell intrinsic excitability in activity deprived cultures compared to control cultures (Fig. 1A). In fact, the rheobase of CA3 pyramidal neurons was reduced in deprived cultures (control: 102.3 ± 7.4 pA, n = 13; deprived: 60 ± 7 pA, n = 12; Mann–Whitney U test: $P < 0.01$; Fig. 1B, Left) and the gain of their input/output curve was increased in deprived cultures (control: 0.109 ± 0.013 spikes/pA, n = 13; deprived: 0.137 ± 0.013 spikes/pA, n = 12; Mann–Whitney U test: $P < 0.05$; Fig. 1B, Right). In order to evaluate the effects of activity deprivation on synaptic transmission, we performed recordings of monosynaptically connected pairs of CA3 pyramidal neurons. The postsynaptic neurons were recorded in voltage clamp (Fig. 1C) or in current clamp (Fig. 1D) and excitatory postsynaptic currents/potentials (EPSCs)/Ps were compared in the two conditions. In deprived organotypic cultures, we found an increase in both EPSC amplitude (control: -25.47 ± 1.98 pA, n = 103; deprived: -34.64 ± 3.93 pA, n = 42, Mann–Whitney U test: $P < 0.05$; Fig. 1C) and EPSP amplitude (control: 1.69 ± 0.23 mV, n = 60; deprived: 3.15 ± 0.74 pA, n = 23, Mann–Whitney U test: $P < 0.05$; Fig. 1D) at synapses between CA3 pyramidal neurons. Contrary to previously reported results (20), we did not find a significant decrease in the connectivity between CA3 pyramidal neurons in deprived cultures (control: 48% of connected pairs among 341 tested pairs; deprived: 39% of connected pairs among 165 tested pairs, $\chi 2$ test: $P > 0.05$; SI Appendix, Fig. S1). We conclude that chronic activity deprivation induces homeostatic compensations of both intrinsic excitability and synaptic transmission in the hippocampal CA3 circuit.

Reduced Axonal Kv1.1 Channel Density in Activity-Deprived Cultures.

It was previously shown that a kynurenate treatment for 2 to 3 d decreases ID current in CA3 pyramidal neurons (3). Kv1.1 channels are highly concentrated at the axon initial segment (AIS), where the AP is initiated. The AIS is structurally supported by specific expression of the scaffold protein Ankyrin G, which also anchors Nav and Kv7 channels. Therefore, we performed coimmunostaining of Kv1.1 channels and Ankyrin G in control and activity-deprived cultures (Fig. 2). In control cultures, Kv1.1 channels staining colocalized with Ankyrin G in the distal part of the AIS of CA3 pyramidal neurons (Fig. 2A). In deprived cultures, we found a +140% increase in the Kv1.1 channels staining in the somatic compartment (Mann–Whitney U test: $P < 0.01$; Fig. 2 A and B and SI Appendix, Fig. S2A) and a -45% decrease in Kv1.1 channels staining in the AIS (Mann–Whitney U test: $P < 0.0001$; Fig. 2A–C and SI Appendix, Fig. S2B). A detailed analysis of the data in 2-µm confocal sections revealed that the somatic increase of Kv1.1 channels in deprived cultures was mostly intracellular (SI Appendix, Fig. S2 C and D). Moreover, we found a +40% increase of AIS length in deprived cultures (control: 30.0 ± 0.3 µm, n = 100; deprived: 42.2 ± 0.4 µm, n = 100; Mann–Whitney U test: $P < 0.0001$; Fig. 2D and SI Appendix, Fig. S2E). However, we did not find any modification in AIS position in deprived cultures. We conclude that chronic activity deprivation leads to a decrease in Kv1.1 channel density at the AIS and an increase of AIS length in CA3 pyramidal neurons (Fig. 2E).

Increased Excitability Is Due to Reduction in Axonal Kv1.1 Channels.

To determine whether the excitability increase in deprived cultures is due to axonal Kv1.1 channel density decrease, we bath applied DTX-K, a Kv1.1 channel blocker. Kv1.1 channel blockade led to a larger increase in excitability in CA3 pyramidal neurons from control cultures than from deprived cultures (Fig. 3 A and B). In fact, the rheobase reduction following DTX-K application was larger in control cultures than in deprived cultures (control: -46.7 ± 9.4 pA, n = 9; deprived: -19 ± 5.7 pA, n = 10; Mann–Whitney U test: $P < 0.05$; Fig. 3B, Left). However, DTX-K application led to a similar increase in the input/output curve gain in control cultures and in deprived cultures (control: 0.105 ± 0.039 pA, n = 9; deprived: 0.072 ± 0.015 pA, n = 10; Mann–Whitney U test: $P > 0.1$; Fig. 3B, Right). Importantly, the intrinsic excitability of CA3 pyramidal neurons was similar in control and deprived cultures after DTX-K application (SI Appendix, Fig. S3A). In fact, the rheobase was similar in control and deprived cultures after DTX-K application (control: 54.4 ± 9.3 pA, n = 9; deprived: 41.0 ± 6.2 pA, n = 10; Mann–Whitney U test: $P > 0.1$; SI Appendix, Fig. S3B). Similarly, the input/output curve gain was similar in control and deprived cultures after DTX-K application (control: 0.224 ± 0.042 pA, n = 9; deprived: 0.212 ± 0.018 pA, n = 10; Mann–Whitney U test: $P > 0.1$; SI Appendix, Fig. S3B). We conclude that the homeostatic increase in excitability in deprived neurons is due to the down-regulation of Kv1.1 channels. Immunostaining of Kv1.1 showed a strong decrease in Kv1.1 staining at the AIS of CA3 pyramidal neurons in deprived cultures (Fig. 2). Moreover, it has been previously shown that axonal Kv1.1 channels are a major determinant of CA3 pyramidal neuron intrinsic excitability (49). To directly test the implication of axonal Kv1.1 channels in homeostatic intrinsic plasticity, we locally blocked Kv1.1 channels by puffing DTX-K on the proximal axon at ∼60 μm from the soma. Interestingly, we found that DTX-K puffing increased excitability of CA3 pyramidal neurons in control but not in deprived cultures (Fig. 3C). In fact, the number of APs elicited by a given current step was increased in control cultures (increase of 3.67 ± 0.32 APs, n = 6; Wilcoxon test: $P < 0.05$) but not in deprived cultures (increase of 0.37 ± 0.46 APs, n = 6; Wilcoxon test: $P > 0.1$). Similarly, the delay of the first spike was reduced by DTX-K puffing in control cultures (-297.8 ± 44.7 ms, n = 6; Wilcoxon test: $P < 0.05$) but not in deprived cultures (+11.4 ± 40.2 ms, n = 6; Wilcoxon test: $P > 0.1$). Finally, the depolarizing slope before the first spike was increased by DTX-K puffing in control cultures (176.3 ± 17.6% of the value before DTX-K puffs, n = 6; Wilcoxon test: $P < 0.05$) but not in deprived cultures (101.9 ± 5% of the value before DTX-K puffs, n = 6; Wilcoxon test: $P > 0.1$) (Fig. 3D). We conclude that the down-regulation of axonal Kv1.1 channels is responsible for the homeostatic increase in excitability in CA3 pyramidal neurons.

Reduction of Kv1.1 Channels Increases Spike Half-Width and Glutamate Release.

Regulation of the density of postsynaptic receptors has been reported in homeostatic synaptic plasticity. However, it has previously been shown that pharmacological blockade of Kv1.1 channels increases release probability at CA3–CA3 synapses via presynaptic AP broadening (45). Therefore, the increase in synaptic transmission observed in deprived cultures (Fig. 1B) can be due to presynaptic axonal Kv1.1 channel down-regulation. First, we calculated the paired pulse ratio (PPR) of synaptic responses at monosynaptically connected CA3 pairs in control and deprived cultures. A significant reduction in the PPR was observed in deprived cultures compared to control cultures (control: 99.5 ± 3.3%, n = 54, deprived: 83.01 ± 2.8%, n = 49, Mann–Whitney U test: $P < 0.001$; Fig. 4A), indicating an increase in glutamate release probability. We conclude that homeostatic synaptic plasticity observed in deprived cultures has a presynaptic component. To determine whether presynaptic Kv1.1 channel downregulation could partly explain the increase in release probability, we tested the effect of DTX-K application on synaptic strength in control and deprived cultures. DTX-K application increased postsynaptic response amplitude in control (118.9 ± 6.0% of the control value, n = 11, Wilcoxon test: $P < 0.05$) but not in deprived cultures (87.4 ± 6.5% of the control value, n = 15; Wilcoxon test: $P > 0.1$; Fig. 4B). Moreover, DTX-K application leads to a decrease in PPR in control (control: 104.6 ± 6.5%, n =

11; control + DTX-K: 83.9 ± 3.6%, n = 11; Wilcoxon test: P < 0.01) but not in deprived cultures (deprived: 86 ± 2.9%, n = 15; deprived + DTX-K: 84.8 ± 4.8%, n = 15; Wilcoxon test: P > 0.1; Fig. 4C). Therefore, the increase in synaptic transmission provoked by Kv1.1 blockade in control cultures is due to an increase in glutamate release. Importantly, DTX-K application in control cultures was sufficient to decrease the PPR down to the value observed in deprived cultures (control + DTX-K: 83.9 ± 3.6%, n = 11; deprived: 86 ± 2.9%, n = 15; Mann–Whitney U test: P > 0.1; Fig. 4C), showing that Kv1.1 down-regulation in deprived cultures is likely to be the cause of the increase in glutamate release. Moreover, in control cultures, we found a strong correlation between the value of the PPR before DTX-K application and the DTX-K–induced decrease in the PPR (SI Appendix, Fig. S4A), indicating that low release probability in control cultures is partly determined by strong presynaptic Kv1.1 expression. This correlation was absent in deprived cultures (SI Appendix, Fig. S4B). We conclude that presynaptic Kv1.1 down-regulation in deprived cultures leads to an increase in glutamate release probability at CA3–CA3 synapses. As Kv1 channels are known to determine synaptic release probability by controlling presynaptic spike width (26, 34, 45), we examined spike waveform in control and deprived cultures. First, we found that the half-width of the somatic spike was larger in deprived cultures than in control cultures (control: 1.33 ± 0.04 ms, n = 80; deprived: 1.66 ± 0.06 ms, n = 47; Mann–Whitney U test: P < 0.001; Fig. 5A). Then, we measured axonal spike half-width using voltage-imaging and axonal cell-attached recordings (Fig. 5 B–D). Due to the limitation of dye diffusion, the voltage-imaging measurements were done at the AIS (34.2 ± 2.4 µm from the soma; control: n = 7; deprived: n = 7), while cell-attached recordings were performed at more distal locations (136.8 ± 17.7 µm from the soma; control: n = 10; deprived: n = 7). Importantly, for axonal cell-attached recordings, we measured the peak-to-peak duration of the signal, which has been shown to be a good approximation of spike half-width (39) (Fig. 5C). In fact, we found no statistical difference in axonal spike half-widths measured in voltage imaging or in cell-attached recordings (SI Appendix, Fig. S5) and therefore we pooled these data. Similar to the somatic spike, we found that the axonal spike was broader in deprived cultures than in control cultures (control: 2.12 ± 0.2 ms, n = 17; deprived: 2.92 ± 0.27 ms, n = 14; Mann–Whitney U test: P < 0.05; Fig. 5D). Altogether, these results suggest that chronic activity deprivation leads to a down-regulation of axonal Kv1.1 channels, inducing a broadening of axonal AP and an increase in glutamate release probability at CA3–CA3 synapses.

Increased Amplitude of Spontaneous mEPSCs but Not Evoked mEPSCs in Deprived Cultures.

To test whether the increase in synaptic strength in deprived cultures is associated with an increase in postsynaptic receptor density, spontaneous miniature excitatory postsynaptic currents (mEPSCs) were recorded in CA3 neurons from control and deprived organotypic cultures. Sodium channel (Nav) dependent spiking was blocked with 1 µM TTX (tetrodotoxin), inhibitory transmission with 100 nM PTX (picrotoxin) and mossy fiber synapses with 1 µM DCG IV ((2S,20R,30R)-2-(20,30 dicarboxycyclopropyl)glycine) to prevent possible contamination of enhanced mEPSC frequency at these synapses (50). An increase in amplitude of spontaneous mEPSCs was found in deprived cultures (136.4%; control: -10.11 ± 0.61 pA, n = 16; deprived cultures: -13.8 ± 0.84 pA, n = 19; Mann–Whitney U test: P < 0.05; Fig. 6A), indicating that postsynaptic AMPAR density was increased in deprived cultures. Furthermore, spontaneous mEPSC frequency was higher in deprived cultures compared to control cultures (Fig. 6A), probably due to an increase in presynaptic vesicle release probability. However, previous studies indicate that the pool of vesicles spontaneously released is different from the one released following spiking (51–54). Some studies even suggest that these two vesicle pools activate different pools of postsynaptic receptors (55, 56). Therefore, the increase in evoked synaptic transmission we measured in deprived cultures (Fig. 1A) may be independent of the observed increase in mEPSC amplitude and frequency (Fig. 6A). To answer this question, we recorded the amplitude of mEPSCs directly evoked by presynaptic spiking. To do so, monosynaptic EPSCs were evoked by

extracellular stimulation in the CA3 pyramidal layer while substituting extracellular Ca2+ with Sr2+ to desynchronize presynaptic release (57). To keep Nav-dependent firing intact, no TTX was present in the bath. Mossy fiber transmission was blocked with 1 μM DCG IV but GABAergic inhibition was left intact to avoid epileptiform activity. Importantly, to avoid the detection of GABAergic events, a low-chloride intracellular solution was used, and neurons were recorded at the Cl- reversal potential (70 mV). The amplitude of the desynchronized synaptic events was measured during the 500 ms following extracellular stimulation (Fig. 6B). These events are due to the desynchronized fusion of single vesicles following the invasion of the presynaptic terminal by an AP (57). We refer to these as evoked mEPSCs. Interestingly, we found no difference in evoked mEPSC amplitude in control and deprived cultures (control: -12.08 ± 1.42 pA, n = 11; deprived: -12.09 ± 0.58 pA, n = 12; Mann–Whitney U test: $P > 0.1$; Fig. 6B). Thus, we found an increase in spontaneous mEPSC amplitude but no difference in evoked mEPSC amplitude in deprived cultures. This raises the possibility that the increase in postsynaptic receptor density does not participate in the homeostatic regulation of synaptic transmission found in deprived cultures.

d-ADF Is Absent in Deprived Cultures.

In CA3 pyramidal neurons, a 10-s somatic subthreshold depolarization inactivates axonal Kv1.1 channels leading to a broadening of the axonal spike and an increase in synaptic release (31, 45). This type of facilitation is named depolarization-induced analog digital facilitation (d-ADF) (46, 58). As axonal Kv1.1 channels are down-regulated in deprived cultures, we could expect a disappearance of d-ADF. We thus examined the depolarization-induced broadening of axonal spikes using voltage-imaging and cell-attached axonal recordings (Fig. 7 A and B). Somatic depolarization from -80 mV to -50 mV for 10 s led to a 30.6% broadening of axonal spike in control cultures (-80 mV: 2.42 ± 0.18 ms, -50 mV: 3.17 ± 0.23 ms, n = 13, Wilcoxon test: $P < 0.01$; Fig. 7C) but had no effect in deprived cultures (-80 mV: 2.92 ± 0.28 ms, -50 mV: 2.88 ± 0.27 ms, n = 14, Wilcoxon test: $P > 0.1$; Fig. 7C). Thus, the axonal spike broadening following subthreshold somatic depolarization is absent in deprived cultures. Next, we tested the increase in glutamate release following subthreshold depolarization by recording from pairs of monosynaptically connected CA3 cells. We depolarized the presynaptic cell resting membrane potential to -50 mV for 10 s. This protocol induced an increase in postsynaptic response amplitude in control cultures (133.9 ± 12.0%, n = 15; Wilcoxon test: $P < 0.001$; Fig. 7C), showing that d-ADF is present at CA3–CA3 synapses. However, in deprived cultures, presynaptic depolarization led to a decrease in synaptic transmission (89.7 ± 2.9% of the control value, n = 13, Wilcoxon test: $P < 0.01$; Fig. 7C). Thus, d-ADF is reversed in deprived cultures. Interestingly, this finding is consistent with a previously published result showing that pharmacological blockade of Kv1.1 channels induces a reversal of d-ADF in control cultures (figure 2 in ref. 45). Therefore, the reversal of d-ADF in deprived cultures is likely to be a consequence of Kv1.1 down-regulation, probably due to the unmasking of Nav inactivation following presynaptic depolarization (59–62). Altogether, these results show that Kv1.1 down-regulation following chronic activity blockade induces the suppression of Kv1.1-dependent increase in axonal spike duration and synaptic transmission induced by somatic depolarization.

Discussion

Our study demonstrates a synergy between homeostatic plasticity of both intrinsic excitability and synaptic transmission in the CA3 network following activity deprivation. This synergy is consistent with the down-regulation of axonal Kv1.1 channels. We report here that the decrease in Kv1.1 channel density at the AIS by ∼50% in deprived cultures was associated with an approximately twofold increase in Kv1.1 channels in the somatic cytoplasm, suggesting an intracellular accumulation of Kv1.1 channels

in the soma, probably due to reduced transport of Kv1.1 channels to the axon. In addition, a 40% increase of AIS length was observed in CA3 pyramidal neurons as previously observed in nucleus magnocellularis (NM) neurons after auditory input deprivation (48). Kv1.1 channels located in the AIS and proximal axon control intrinsic excitability of CA3 pyramidal cells (3, 49), whereas Kv1.1 channels located in presynaptic terminals control presynaptic spike duration and synaptic release (31, 45, 46, 63). Thus, the down-regulation of axonal Kv1.1 channels following chronic activity deprivation leads to the increase in both intrinsic excitability of CA3 neurons and synaptic release probability at CA3–CA3 synapses. Furthermore, Kv1.1 down-regulation reverses d-ADF. In fact, a presynaptic subthreshold depolarization increases synaptic release in control cultures but decreases it in deprived cultures.

Synergistic Homeostatic Regulation of Intrinsic Excitability and Synaptic Transmission.

Various studies have shown a synergy of homeostatic intrinsic and synaptic plasticity in neuronal networks (17, 64, 65). Usually, this synergy is explained by common molecular pathways leading to regulation of different molecular effectors. For example, in dissociated cortical cultures, chronic activity deprivation leads to a diminution of brain-derived neurotrophic factor (BDNF) exocytosis entailing both homeostatic synaptic plasticity through regulation of AMPARs and of homeostatic intrinsic plasticity through regulation of sodium and potassium voltage-gated channels (4, 5, 66). In the CA3 network, chronic activity deprivation has been shown independently to induce homeostatic intrinsic (3) and synaptic plasticity (20). Our data suggest that the increase in glutamate release probability at CA3–CA3 synapses in deprived cultures is due to Kv1.1 down-regulation. Moreover, both somatic and axonal spikes have been found to be broader in deprived cultures compared to control cultures. Therefore, it is likely that the down-regulation of Kv1.1 channels located in the AIS and proximal axon accounts for the increase in excitability, while the downregulation of Kv1.1 channels in presynaptic terminals accounts for the increase in glutamate release via broadening of the presynaptic spike. We thus describe here a significant mechanism underlying homeostatic synaptic plasticity via presynaptic spike waveform modulation, a phenomenon that has been described in neocortical dissociated cultures and at the batrachian neuromuscular junction (36, 38).

Kv1.1 Down-Regulation Is Not the Only Determinant of Homeostatic Plasticity.

In this study, we showed that Kv1.1 down-regulation induces both homeostatic intrinsic and synaptic plasticity following activity deprivation. However, it is likely that Kv1.1 down-regulation is accompanied by other mechanisms of homeostatic plasticity. First, AIS length was found to be increased following kynurenate treatment. Such an increase of AIS length following activity deprivation has been described as a main determinant of homeostatic intrinsic plasticity in several studies (48, 67–71). Therefore, it is likely that the increase in AIS length we found is also involved in the excitability increase observed in CA3 neurons from deprived cultures. Second, homeostatic elevation of excitatory synaptic transmission is often due to up-regulation of postsynaptic AMPA receptors and/or up-regulation of vesicle release probability. We found that spontaneous mEPSC amplitude and frequency recorded in TTX were increased in deprived cultures. Therefore, it is probable that the postsynaptic glutamate receptors and the presynaptic vesicular machinery are also regulated to produce an increase in synaptic strength in deprived cultures. However, it has been shown that spontaneous and evoked synaptic transmission rely on different pools of vesicles and can activate different pools of postsynaptic receptors (51, 52, 55, 56). The substitution of Ca^{2+} by Sr^{2+} allows the measurement of single vesicle fusion events, i.e., evoked mEPSCs. We found no change in evoked mEPSC amplitude in deprived cultures. This raises the possibility that the increase in spontaneous synaptic transmission is due to an increase in postsynaptic receptor density, while the increase in evoked synaptic transmission is due to presynaptic Kv1.1 downregulation. Finally, whether regulation of other types of voltage-gated

channels (such as up-regulation of presynaptic Nav channels) participates in the enhanced synaptic release at deprived synapses cannot be totally discounted.

Comparison with Homeostatic Plasticity Induced by TTX.

Mitra et al. reported an increase in synaptic transmission between CA3 pyramidal cells following chronic activity blockade together with a strong reduction of the connection probability between CA3 neurons (from ∼45% in control cultures to ∼20% in activity deprived cultures) (20). They concluded that the decrease in connectivity prevents the overexcitation of the CA3 network despite the increase in synaptic transmission. We found a much smaller and nonsignificant decrease in connectivity following activity deprivation (48% in control cultures, 39% in deprived cultures). This discrepancy may arise from the difference in the drug used to inhibit activity in the two studies. Mitra et al. (20) used TTX, which blocks spiking, whereas we used kynurenate, which blocks excitatory synaptic transmission. In their study, Mitra et al. show that the decrease in connectivity is due to an increase in the binding between CDK5 and p25/p35, which is known to silence synapses. Interestingly, they did not observe this CDK5 up-regulation following activity deprivation with a blocker of excitatory transmission, NBQX (2,3-dioxo-6-nitro-1,2,3,4-tetrahydrobenzo[f]quinoxaline-7-sulfonamide). Thus, homeostatic synaptic plasticity following activity deprivation by AP blockade (TTX) or excitatory transmission blockade (kynurenate or NBQX) appears to involve different molecular actors (12, 15, 72).

Overexcitation Dampening through Reversion of d-ADF.

In pairs of connected CA3 pyramidal neurons, a long subthreshold depolarization preceding the spikes (5 to 10 s at 50 mV) inactivates axonal Kv1.1 channels, broadens presynaptic spike, and increases synaptic transmission (which produces d-ADF). Thus, a local excitation of the network will be amplified through this phenomenon. In activity-deprived cultures, we showed that Kv1.1 channels are down-regulated and d-ADF is reversed. In this case, we suppose that the reduction of Kv1.1 channels unmasks the Nav channel inactivation by subthreshold depolarization, leading to a decrease in presynaptic spike amplitude and synaptic strength (59, 61, 62). This hypothesis will need more experiments to be confirmed. Interestingly, the reversal of d-ADF will tend to dampen overexcitation in the CA3 network as a global depolarization will diminish synaptic transmission. Thus, this phenomenon could be a mechanism mitigating overexcitation in deprived cultures despite the global increase in intrinsic excitability and synaptic strength. According to this point of view, down-regulation of Kv1.1 channels following activity deprivation would allow a homeostatic increase in network activity while avoiding pathological states.

Voltage-Gated Channels as Regulators of Synaptic Transmission.

Classically, the role of voltage-gated channels is limited to the modulation of neuronal intrinsic excitability. However, numerous studies have shown that short-term inactivation of Kv channels by resting membrane potential depolarization broadens the presynaptic AP and therefore increases synaptic release (25, 26, 28, 34, 35, 45). Here, we show that long-term down-regulation of Kv1.1 channels causes a broadening of presynaptic spikes and an increase in synaptic transmission. Thus, neuronal networks can exhibit long-term plasticity of the AP waveform. Moreover, sodium channel availability is also a determinant of spike waveform and synaptic transmission (27, 46, 62, 73). Therefore, we could expect that homeostatic intrinsic plasticity via Nav regulation (2, 5, 6, 8) may also impact synaptic transmission. In conclusion, regulation of axonal voltage-gated channels could allow neurons to modulate efficiently intrinsic excitability and synaptic transmission.

Methods

Organotypic Hippocampal Slice Cultures.

Our experiments were conducted according to the European and Institutional guidelines (Council Directive 86/609/EEC and French National Research Council and approved by the local health authority [Préfecture des Bouches-du-Rhône, Marseille]). Hippocampal slice cultures were prepared using an interface technique (74, 75). Briefly, postnatal day 5 to 7 Wistar rats were deeply anesthetized by intraperitoneal injection of chloral hydrate, the brain was removed, and each hippocampus was individually dissected. Hippocampal slices (300 µm) were placed on 20-mm latex membranes (Millicell) inserted into 35-mm Petri dishes containing 1 mL of culture medium and maintained for up to 12 d in an incubator at 34 °C, 95% O2–5% CO2. The culture medium contained (in milliliters) 25Minimal Essential Medium, 1.25 Hank's Balanced Salt Solution, 12.5 horse serum, 0.5 penicillin/streptomycin, 0.8 glucose (1 M), 0.1 ascorbic acid (1 mg/mL), 0.4 Hepes (1 M), 0.5 B27, and 8.95 sterile H2O. To arrest glial proliferation, 5 µMAra-C (cytarabine) was added for one night to the culture medium after 3 DIV.

Solutions and Pharmacology.

The control perfusion solution contained (in millimoles) 125 NaCl, 26 NaHCO3, 3 CaCl2, 2.5 KCl, 2 MgCl2, 0.8 NaH2PO4, and 10 D-glucose and was continuously equilibrated with 95% O2–5% CO2. Patch pipettes (6 to 9 MΩ) were filled with a solution containing (in millimoles) 120 K-gluconate, 20 KCl, 10 Hepes, 0.5 EGTA (ethylene glycol-bis(β-aminoethyl ether)-N,N,N0,N0-tetraacetic acid), 2 Na2ATP, 0.3 NaGTP, and 2 MgCl2, pH 7.4. All drugs were applied via the bath solution. D-type currents (Kv1 channels) were blocked by bath application of DTX-K (50 to 100 nM; Sigma), a blocker of Kv1.1 channels. To chronically block excitatory transmission, 2mMkynurenate was added to the culture medium at 2 or 3 d before recordings; recordings of treated cultures were performed 7 to 12 DIV.

Paired Recordings and Analysis.

Dual recordings from pairs of neurons were obtained as previously described (74). The external saline contained (in millimoles): 125 NaCl, 26 NaHCO3, 3 CaCl2, 2.5 KCl, 2 MgCl2, 0.8 NaH2PO4 and 10 D-glucose, and was equilibrated with 95% O2–5% CO2. Patch pipettes (5 to 10 MO) were pulled from borosilicate glass and filled with an intracellular solution containing (in millimoles): 120 K gluconate, 20 KCl, 10 Hepes, 0.5 EGTA, 2 MgCl2, 2Na2ATP, and 0.3 NaGTP (pH 7.4). Recordings were performed at 30°C in a temperature-controlled recording chamber (Luigs & Neumann). Usually, the presynaptic neuron was recorded in current clamp and the postsynaptic cell in voltage clamp. Both pre- and postsynaptic cells were held at their resting membrane potential (approximately 65 mV). Presynaptic APs were generated by injecting brief (5 ms) depolarizing pulses of current at a frequency of 0.1 Hz. PPR was assessed with two presynaptic stimulations (150-ms interval). Voltage and current signals were low-pass filtered (3 kHz), and sequences (200 to 500 ms) were acquired at 10 to 20 kHz with pClamp (Axon Instruments, Molecular Devices) version 10. Electrophysiological signals were analyzed with ClampFit (Axon Instruments) and custom-made software was written in LabView (National Instruments). Postsynaptic responses could be averaged following alignment of the presynaptic APs using automatic peak detection. The presence or absence of a synaptic connection was determined on the basis of averages of 20 individual traces.

mEPSC Recordings and Analysis.

In spontaneous mEPSC experiments, inhibitory synaptic transmission, Nav channels, and mossy fiber synapses were blocked using, respectively, 100 nM PTX, 1 µM TTX, and 1 µM DCG-IV (mGluR2 agonist). In evoked mEPSC experiments, only mossy fiber synapses were blocked using 1 µM DCG-IV. To induce desynchronization of evoked synaptic transmission, Ca2+ was replaced by Sr2+ in extracellular solution. To avoid the detection of GABAergic events in this experiment we used a low-chloride

intracellular solution (in millimoles: 150 K gluconate, 4.6 KCl, 10 Hepes, 0.5 EGTA, 2MgCl2, 2 Na2ATP, and 0.3 NaGTP, 10 phosphocreatine), and we recorded the neurons at the Cl- reversal potential (70 mV in this case). Spontaneous and evoked mEPSCs were selected by hand using ad hoc analysis software written in Lab-View (National Instruments). Then the traces were exported in ClampFit (Axon Instruments) to analyze the amplitude and interevent intervals.

Axonal Cell-Attached Recordings.

Simultaneous recordings from the soma in whole-cell configuration and the axon in cell-attached configuration were obtained from CA3 pyramidal neurons. Briefly, CA3 pyramidal cells were recorded with 50 μM Alexa 488 (Invitrogen) in the recording solution. Following whole-cell access of the somatic compartment, we waited 10 to 15 min to allow the dye to strongly stain the axonal compartment and visualized the cell at 488 nm with a LSM-710 confocal microscope (Zeiss). The axon was identified by visual clues: a thin, aspiny process emerging from the soma or a proximal dendrite. We approached a second pipette containing extracellular solution to the desired axonal target and brief suction was applied to the pipette. Under these conditions, the spike measured in the axon had a positive polarity (amplitude 0.3 to 1.2 mV) when recorded in current clamp.

Puff Applications.

CA3 neurons were filled with 50 μM Alexa 488 (Invitrogen) to visualize neuronal morphology. Neurons were recorded for ∼10 min before imaging with a LSM-710 confocal system (Zeiss). Alexa 488 was excited with laser source at 488 nm. The axon was identified by visual clues: a thin, aspiny process emerging from the soma or a proximal dendrite. Localized puffs of Kv1.1 channel blocker were applied on the AIS of the recorded neuron with a patch pipette filled with a solution containing extracellular saline with 50 μM Alexa 594 (Invitrogen) and 100 nM DTX-K (Sigma). Alexa 594 was excited with a laser source at 543 nm. Short puffs (20 to 50 ms, 5 psi) were ejected every 10 s with a Toohey Spritzer pressure system (Toohey Company).

Voltage Imaging of the Axon.

CA3 pyramidal neurons were imaged with JPW3028 (250 μM) following a protocol detailed in ref. 44. JPW3028 was a gift from L. M. Loew, University of Connecticut Health Center, Farmington, CT. In practice, the tip of the electrode was prefilled with Alexa 488 (50 μM) to visualize the morphology of the neuron and back filled with the voltage-sensitive dye JPW3028 (250 μM). After 5 min of whole-cell recording, Alexa diffused into the neuron and the neuronal morphology was acquired with the LSM-710 confocal microscope. If the neuron displayed a clearly visible axon and axon initial segment (AIS), the protocol was continued (otherwise the cell was discarded). The AIS was defined as the proximal segment of the axon extending up to 60 μm from the axon hillock in CA3 pyramidal neurons (76). The cell was recorded in whole-cell mode for at least 25 min to obtain sufficient diffusion of the dye into the axon, and the imaging protocol was then started. The cell was illuminated in wide field with a 525-nm LED system (CoolLed; Roper Scientific/Photometrics) via a 60 × 1.0 numerical aperture water-immersion objective (Zeiss). Collected fluorescence was long-pass filtered at 610 nm and projected onto a 128 × 128 pixel high-speed EMCCD camera (Evolve 128; Photometrics) with a maximum frame rate of 7 kHz. In a typical trial, we induced APs in the soma by injecting a 5- to 10-ms current pulse, synchronized with LED illumination, and camera acquisition at 500 Hz for 40 ms. To improve the signal-to-noise ratio, we acquired 50 to 100 sweeps sequentially and reconstructed the signal at 1 to 2 kHz by a shift and mean algorithm (77). All these operations were performed using ad hoc analysis software written in LabView (National Instruments).

Immunohistochemistry.

Control and activity-deprived hippocampal organotypic cultures were fixed in 4% paraformaldehyde for 30 min and washed in phosphate buffered saline (PBS). Immunodetection was done in free-floating sections. Brain slices were treated with 50 mM NH4Cl for 30 min and incubated in blocking buffer (10% goat serum, 0.1% Triton X-100 in PBS) for 2 h to avoid nonspecific binding. Slices were incubated overnight at 4 °C with the primary antibodies diluted in incubation buffer (PBS, 1% goat serum and 0.1% Triton X-100). The primary antibodies used were: mouse IgG2b anti-Kv1.1 (1:100, Neuromab K36/15) and mouse IgG2a anti-ankyrinG (1:100, Neuromab N106/36). After extensive washing in incubation buffer, the secondary antibodies, Alexa 568 goat anti-mouse IgG2a (1:500) and Alexa 488 goat anti-mouse IgG2b (1:500) were incubated for 2 h at room temperature and then washed. Bisbenzimide (1:2,500) was added for 3 min to stain nuclei and identify hippocampal formation domains. After staining, the coverslips were mounted with Fluoromount-G (SouthernBiotech) and the images were acquired on a confocal microscope (Leica SP5) using the same parameters to compare intensities between control and experimental conditions. Briefly, all confocal images were acquired at 1-µm z axis steps and with a 1,024 × 1,024 pixel resolution. Image stacks were converted into single maximum intensity z axis projections using ImageJ/Fiji software. Images were prepared for presentation using Adobe CS4 software.

Immunochemistry Image Analysis and Statistics.

Kv1.1 fluorescence intensity was analyzed using ImageJ/Fiji software in the AIS and neuronal somas from 11 control and 11 treated brain slices obtained from three independent experiments. On each AIS, a five-pixel line was drawn along the Kv1.1 staining to obtain fluorescence integrated density. Potential background differences in brain slices were taken into account and subtracted from the integrated density value to obtain corrected total fluorescence (CTF), using the following formula: CTF = Kv1.1 integrated density (Kv1.1 area × mean fluorescence of background readings). Data were acquired from at least 10 AISs in each control or treated slice. To quantify Kv1.1 fluorescence intensity in the somas of CA3 neurons, a polygon containing the soma area based on nuclei staining in the z axis maximum projection was drawn. Then, integrated density was obtained and background activity subtracted to obtain CTF, as described above. Somatic Kv1.1 intensity was also measured in images containing two confocal sections (2 µm), at the level of the nucleus, drawing a line crossing the soma and nucleus and to obtain the Kv1.1 fluorescence profile. AIS length was measured, as previously described and standardized (78), using ankyrinG staining. Briefly, a line was drawn starting from each soma down to its axon following the ankyrinG staining. This defines a fluorescence intensity profile along the AIS that increases and then decreases. Starting and end positions of the AIS are defined as the positions where ankyrinG intensity crosses 33% of the maximum intensity point measured in each ankyrinG profile.

Statistical Tests.

The results are presented as the mean ± SEM. Statistical differences between experimental conditions were calculated, not assuming Gaussian distributions or equal variances, using the Mann–Whitney U test or Wilcoxon rank-signed test. For analysis of the connectivity, we used an $\chi 2$ test.

ACKNOWLEDGMENTS.

This work was supported by INSERM, CNRS (to D.D.), Ecole Normal Superieure (doctoral grant to M.Z.), Agence Nationale de la Recherche (REPREK ANR-11-BSV16-016-01 to D.D.; LoGIK ANR-17-CE16-022), Fondation pour la Recherche M edicale (doctoral grant to M.Z. FDT-2015-0532147 and DVS-2013-1228768 and DEQ20180839583 to D.D.), and Ministerio de Ciencia y Universidades (RTI2018-095156-

B-100 to J.J.G.). We thank Prof. U. Gerber, Prof. P. Jonas, and Dr. R. Brette for helpful comments on the manuscript.

References

1. G. Turrigiano, Too many cooks? Intrinsic and synaptic homeostatic mechanisms in cortical circuit refinement. Annu. Rev. Neurosci. 34, 89–103 (2011).
2. C.O.Aptowicz, P. E. Kunkler, R. P. Kraig, Homeostatic plasticity in hippocampal slice cultures involves changes in voltage-gated Na+ channel expression. Brain Res. 998, 155–163 (2004).
3. R. H. Cudmore, L. Fronzaroli-Molinieres, P. Giraud, D. Debanne, Spike-time precision and network synchrony are controlled by the homeostatic regulation of the D-type potassium current. J. Neurosci. 30, 12885–12895 (2010).
4. N. S. Desai, L. C. Rutherford, G. G. Turrigiano, BDNF regulates the intrinsic excitability of cortical neurons. Learn. Mem. 6, 284–291 (1999).
5. N. S. Desai, L. C. Rutherford, G. G. Turrigiano, Plasticity in the intrinsic excitability of cortical pyramidal neurons. Nat. Neurosci. 2, 515–520 (1999).
6. H. E. Driscoll, N. I.Muraro, M. He, R. A. Baines, Pumilio-2 regulates translation of Nav1.6 to mediate homeostasis of membrane excitability. J. Neurosci. 33, 9644–9654 (2013).
7. C. Gasselin, Y. Inglebert, D. Debanne, Homeostatic regulation of h-conductance controls intrinsic excitability and stabilizes the threshold for synaptic modification in CA1 neurons. J. Physiol. 593, 4855–4869 (2015).
8. K. G. Pratt, C. D. Aizenman, Homeostatic regulation of intrinsic excitability and synaptic transmission in a developing visual circuit. J. Neurosci. 27, 8268–8277 (2007).
9. I. van Welie, J. A. van Hooft, W. J. Wadman, Background activity regulates excitability of rat hippocampal CA1 pyramidal neurons by adaptation of a K+ conductance. J.Neurophysiol. 95, 2007–2012 (2006).
10. E. C. Beattie et al., Control of synaptic strength by glial TNF alpha. Science 295, 2282–2285 (2002).
11. Q. Hou, D. Zhang, L. Jarzylo, R. L. Huganir, H.-Y. Man, Homeostatic regulation of AMPA receptor expression at single hippocampal synapses. Proc. Natl. Acad. Sci.U.S.A. 105, 775–780 (2008).
12. K. Ibata, Q. Sun, G. G. Turrigiano, Rapid synaptic scaling induced by changes in postsynaptic firing. Neuron 57, 819–826 (2008).
13. S. K. Jakawich et al., Local presynaptic activity gates homeostatic changes in presynaptic function driven by dendritic BDNF synthesis. Neuron 68, 1143–1158 (2010).
14. D. Stellwagen, R. C. Malenka, Synaptic scaling mediated by glial TNF-alpha. Nature 440, 1054–1059 (2006).
15. M. A. Sutton et al., Miniature neurotransmission stabilizes synaptic function via tonic suppression of local dendritic protein synthesis. Cell 125, 785–799 (2006).
16. T. C. Thiagarajan, M. Lindskog, R. W. Tsien, Adaptation to synaptic inactivity in hippocampal neurons. Neuron 47, 725–737 (2005).
17. C. J. Wierenga, K. Ibata, G. G. Turrigiano, Postsynaptic expression of homeostatic plasticity at neocortical synapses. J. Neurosci. 25, 2895–2905 (2005).
18. S. H. Kim, T. A. Ryan, CDK5 serves as a major control point in neurotransmitter release. Neuron 67, 797–809 (2010).
19. V. Lazarevic, S. Pothula, M. Andres-Alonso, A. Fejtova, Molecular mechanisms driving homeostatic plasticity of neurotransmitter release. Front. Cell. Neurosci. 7, 244 (2013).
20. A. Mitra, S. S. Mitra, R.W. Tsien, Heterogeneous reallocation of presynaptic efficacy in recurrent excitatory circuits adapting to inactivity. Nat. Neurosci. 15, 250–257 (2011).

21. R. Begum, Y. Bakiri, K. E. Volynski, D. M. Kullmann, Action potential broadening in a presynaptic channelopathy. Nat. Commun. 7, 12102 (2016).
22. S. Boudkkazi, L. Fronzaroli-Molinieres, D. Debanne, Presynaptic action potential waveform determines cortical synaptic latency. J. Physiol. 589, 1117–1131 (2011).
23. M. Carta et al., Membrane lipids tune synaptic transmission by direct modulation of presynaptic potassium channels. Neuron 81, 787–799 (2014).
24. J. R. Geiger, P. Jonas, Dynamic control of presynaptic Ca(2+) inflow by fast-inactivating K(+) channels in hippocampal mossy fiber boutons. Neuron 28, 927–939 (2000).
25. S. Kim, Action potential modulation in CA1 pyramidal neuron axons facilitates OLM interneuron activation in recurrent inhibitory microcircuits of rat hippocampus. PLoS One 9, e113124 (2014).
26. M. H. P. Kole, J. J. Letzkus, G. J. Stuart, Axon initial segment Kv1 channels control axonal action potential waveform and synaptic efficacy. Neuron 55, 633–647 (2007).
27. S. Rama et al., Presynaptic hyperpolarization induces a fast analogue modulation of spike evoked transmission mediated by axonal sodium channels. Nat. Commun. 6, 10163 (2015).
28. M. J. M. Rowan, J. M. Christie, Rapid state-dependent alteration in Kv3 channel availability drives flexible synaptic signaling dependent on somatic subthreshold depolarization. Cell Rep. 18, 2018–2029 (2017).
29. M. J. M. Rowan, G. DelCanto, J. J. Yu, N. Kamasawa, J. M. Christie, Synapse-level determination of action potential duration by K(+) channel clustering in axons. Neuron 91, 370–383 (2016).
30. T. Sasaki, N. Matsuki, Y. Ikegaya, Action-potential modulation during axonal conduction. Science 331, 599–601 (2011).
31. T. Sasaki, N. Matsuki, Y. Ikegaya, Effects of axonal topology on the somatic modulation of synaptic outputs. J. Neurosci. 32, 2868–2876 (2012).
32. C. Saviane, M. H. Mohajerani, E. Cherubini, An ID-like current that is downregulated by Ca2+ modulates information coding at CA3-CA3 synapses in the rat hippocampus. J. Physiol. 552, 513–524 (2003).
33. Y. Shu, A. Hasenstaub, A. Duque, Y. Yu, D. A.McCormick, Modulation of intracortical synaptic potentials by presynaptic somatic membrane potential. Nature 441, 761–765 (2006).
34. Y. Shu, Y. Yu, J. Yang, D. A. McCormick, Selective control of cortical axonal spikes by a slowly inactivating K+ current. Proc. Natl. Acad. Sci. U.S.A. 104, 11453–11458 (2007).
35. U. Vivekananda et al., Kv1.1 channelopathy abolishes presynaptic spike width modulation by subthreshold somatic depolarization. Proc.Natl.Acad. Sci.U.S.A. 114, 2395–2400 (2017).
36. M. B. Hoppa, G. Gouzer,M. Armbruster, T. A. Ryan, Control and plasticity of the presynaptic action potential waveform at small CNS nerve terminals. Neuron 84, 778–789 (2014).
37. B. Li et al., Neuronal inactivity co-opts LTP machinery to drive potassium channel splicing and homeostatic spike widening. Cell 181, 1547–1565.e15 (2020).
38. T. A. Nick, A. B. Ribera, Synaptic activity modulates presynaptic excitability. Nat. Neurosci. 3, 142–149 (2000).
39. A. Ritzau-Jost et al., Large, stable spikes exhibit differential broadening in excitatory and inhibitory neocortical boutons. Cell Rep. 34, 108612 (2021).
40. J. F. Storm, Temporal integration by a slowly inactivating K+ current in hippocampal neurons. Nature 336, 379–381 (1988).
41. G. W. Crabtree et al., Alteration of neuronal excitability and short-term synaptic plasticity in the prefrontal cortex of a mouse model of mental illness. J. Neurosci. 37, 4158–4180 (2017).
42. E. M. Goldberg et al., K+ channels at the axon initial segment dampen near-threshold excitability of neocortical fast-spiking GABAergic interneurons. Neuron 58, 387–400 (2008).
43. I. H. Cho et al., The potassium channel subunit Kvβ1 serves as a major control point for synaptic facilitation. Proc. Natl. Acad. Sci. U.S.A. 117, 29937–29947 (2020).

44. A. J. Foust, Y. Yu, M. Popovic, D. Zecevic, D. A. McCormick, Somatic membrane potential and Kv1 channels control spike repolarization in cortical axon collaterals and presynaptic boutons. J. Neurosci. 31, 15490–15498 (2011).
45. A. Bialowas et al., Analog modulation of spike-evoked transmission in CA3 circuits is determined by axonal Kv1.1 channels in a time-dependent manner. Eur. J. Neurosci.41, 293–304 (2015).
46. M. Zbili, D. Debanne, Past and future of analog-digital modulation of synaptic transmission. Front. Cell. Neurosci. 13, 160 (2019).
47. F. Kirchheim, S. Tinnes, C. A. Haas,M. Stegen, J. Wolfart, Regulation of action potential delays via voltage-gated potassium Kv1.1 channels in dentate granule cells during hippocampal epilepsy. Front. Cell. Neurosci. 7, 248 (2013).
48. H. Kuba, R. Yamada, G. Ishiguro, R. Adachi, Redistribution of Kv1 and Kv7 enhances neuronal excitability during structural axon initial segment plasticity. Nat. Commun. 6, 8815 (2015).
49. S. Rama et al., The role of axonal Kv1 channels in CA3 pyramidal cell excitability. Sci. Rep. 7, 315 (2017).
50. J. Kim, R. W. Tsien, Synapse-specific adaptations to inactivity in hippocampal circuits achieve homeostatic gain control while dampening network reverberation. Neuron 58, 925–937 (2008).
51. N. L. Chanaday, E. T. Kavalali, Presynaptic origins of distinct modes of neurotransmitter release. Curr. Opin. Neurobiol. 51, 119–126 (2018).
52. E. T. Kavalali, The mechanisms and functions of spontaneous neurotransmitter release. Nat. Rev. Neurosci. 16, 5–16 (2015).
53. E. T. Kavalali et al., Spontaneous neurotransmission: An independent pathway for neuronal signaling? Physiology (Bethesda) 26, 45–53 (2011).
54. D. M. Ramirez, E. T. Kavalali, Differential regulation of spontaneous and evoked neurotransmitter release at central synapses. Curr. Opin. Neurobiol. 21, 275–282 (2011).
55. D. Atasoy et al., Spontaneous and evoked glutamate release activates two populations of NMDA receptorswith limited overlap. J. Neurosci. 28, 10151–10166 (2008).
56. Y. Sara, M. Bal, M. Adachi, L. M. Monteggia, E. T. Kavalali, Use-dependent AMPA receptor block reveals segregation of spontaneous and evoked glutamatergic neurotransmission. J. Neurosci. 31, 5378–5382 (2011).
57. M. A. Xu-Friedman, W. G. Regehr, Probing fundamental aspects of synaptic transmission with strontium. J. Neurosci. 20, 4414–4422 (2000).
58. D. Debanne, A. Bialowas, S. Rama, What are the mechanisms for analogue and digital signalling in the brain? Nat. Rev. Neurosci. 14, 63–69 (2013).
59. T. Hori, T. Takahashi, Mechanisms underlying short-term modulation of transmitter release by presynaptic depolarization. J. Physiol. 587, 2987–3000 (2009).
60. P. F. Kramer, E. L. Twedell, J. H. Shin, R. Zhang, Z. M. Khaliq, Axonal mechanisms mediating γ-aminobutyric acid receptor type A (GABA-A) inhibition of striatal dopamine release. eLife 9, e55729 (2020).
61. A. Takeuchi, N. Takeuchi, Electrical changes in pre- and postsynaptic axons of the giant synapse of Loligo. J. Gen. Physiol. 45, 1181–1193 (1962).
62. M. Zbili et al., Axonal Na+ channels detect and transmit levels of input synchrony in local brain circuits. Sci. Adv. 6, eaay4313 (2020).
63. S. Rama, M. Zbili, D. Debanne, Modulation of spike-evoked synaptic transmission: The role of presynaptic calcium and potassium channels. Biochim. Biophys. Acta 1853, 1933–1939 (2015).
64. J. Echegoyen, A. Neu, K. D. Graber, I. Soltesz, Homeostatic plasticity studied using in vivo hippocampal activity-blockade: Synaptic scaling, intrinsic plasticity and age dependence. PLoS One 2, e700 (2007).

65. M. E. Lambo, G. G. Turrigiano, Synaptic and intrinsic homeostatic mechanisms cooperate to increase L2/3 pyramidal neuron excitability during a late phase of critical period plasticity. J. Neurosci. 33, 8810–8819 (2013).
66. L. C. Rutherford, S. B. Nelson, G. G. Turrigiano, BDNF has opposite effects on the quantal amplitude of pyramidal neuron and interneuron excitatory synapses. Neuron 21, 521–530 (1998).
67. S. Goethals, R. Brette, Theoretical relation between axon initial segment geometry and excitability. eLife 9, e53432 (2020).
68. N. Jamann et al., Sensory input drives rapid homeostatic scaling of the axon initial segment in mouse barrel cortex. Nat. Commun. 12, 23 (2021).
69. S.A.Booker et al., Input-output relationship of CA1 pyramidal neurons reveals intact homeostatic mechanisms in a mouse model of fragile X syndrome. Cell Rep. 32, 107988 (2020).
70. R. Yamada, H. Kuba, Structural and functional plasticity at the axon initial segment. Front. Cell. Neurosci. 10, 250 (2016).
71. H. Kuba, Y. Oichi, H. Ohmori, Presynaptic activity regulates Na(+) channel distribution at the axon initial segment. Nature 465, 1075–1078 (2010).
72. A. Bacci et al., Chronic blockade of glutamate receptors enhances presynaptic release and downregulates the interaction between synaptophysin-synaptobrevin-vesicle associated membrane protein 2. J. Neurosci. 21, 6588–6596 (2001).
73. S.-Y. Kawaguchi, T. Sakaba, Control of inhibitory synaptic outputs by low excitability of axon terminals revealed by direct recording. Neuron 85, 1273–1288 (2015).
74. D. Debanne et al., Paired-recordings from synaptically coupled cortical and hippocampal neurons in acute and cultured brain slices. Nat. Protoc. 3, 1559–1568 (2008).
75. L. Stoppini, P. A. Buchs, D. Muller, A simple method for organotypic cultures of nervous tissue. J. Neurosci. Methods 37, 173–182 (1991).
76. J. P. Meeks, S. Mennerick, Action potential initiation and propagation in CA3 pyramidal axons. J. Neurophysiol. 97, 3460–3472 (2007).
77. S. Rama, Shift and mean algorithm for functional imaging with high spatio-temporal resolution. Front. Cell. Neurosci. 9, 446 (2015).
78. M. S. Grubb, J. Burrone, Activity-dependent relocation of the axon initial segment fine-tunes neuronal excitability. Nature 465, 1070–1074 (2010).

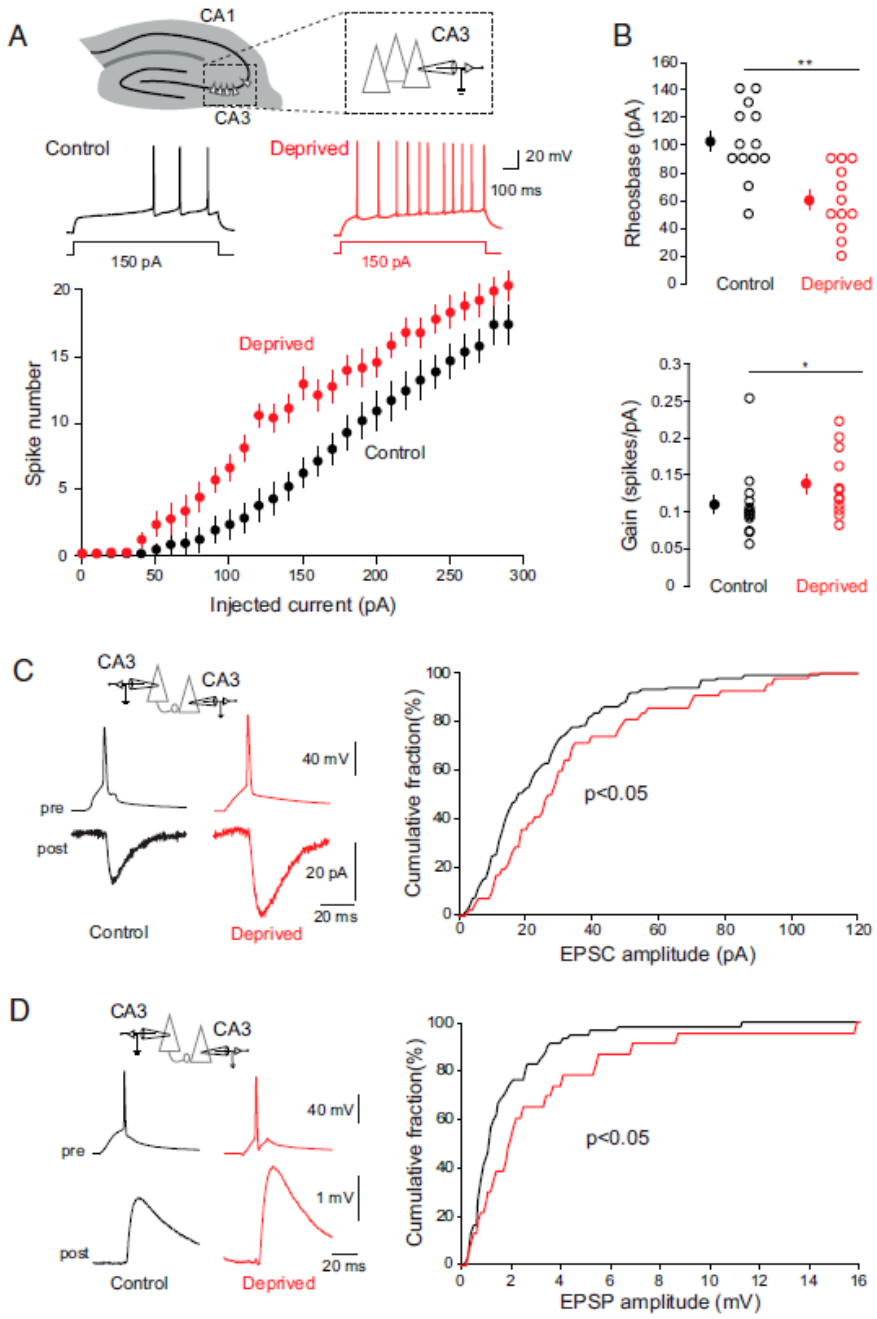

Fig. 1. Increased excitability and synaptic transmission in the CA3 circuit following chronic activity deprivation. (A) Increase in excitability in activity deprived cultures (red) compared to control cultures (black). Top, Example current-clamp traces recorded in CA3 pyramidal neurons in control (black) and in deprived (red) cultures. Bottom, Average data across groups. CA3 pyramidal neurons display a larger excitability in deprived cultures (red; n = 13) than in control cultures (black; n = 12). (B) Top, Reduced rheobase in deprived cultures (red) compared to control cultures (black). Bottom, Increased input/output curve gain in deprived cultures (red) compared to control cultures (black). *P < 0.05, **P < 0.01. (C and D) Increase in synaptic strength in deprived cultures (red) compared to control cultures (black). (C) Left, Examples of CA3–CA3 EPSCs in control and deprived cultures (average of 30 traces). Right, Cumulative histogram of EPSC amplitude in control (black) and deprived (red) cultures. Note the rightward shift for deprived cultures showing a global increase in EPSC amplitude. (D) Left, Examples of CA3–CA3 EPSPs in control and deprived cultures (average of 30 traces). Right, Cumulative histogram of EPSP amplitude in control (black) and deprived (red) cultures. Note the rightward shift for deprived cultures showing a global increase in EPSP amplitude.

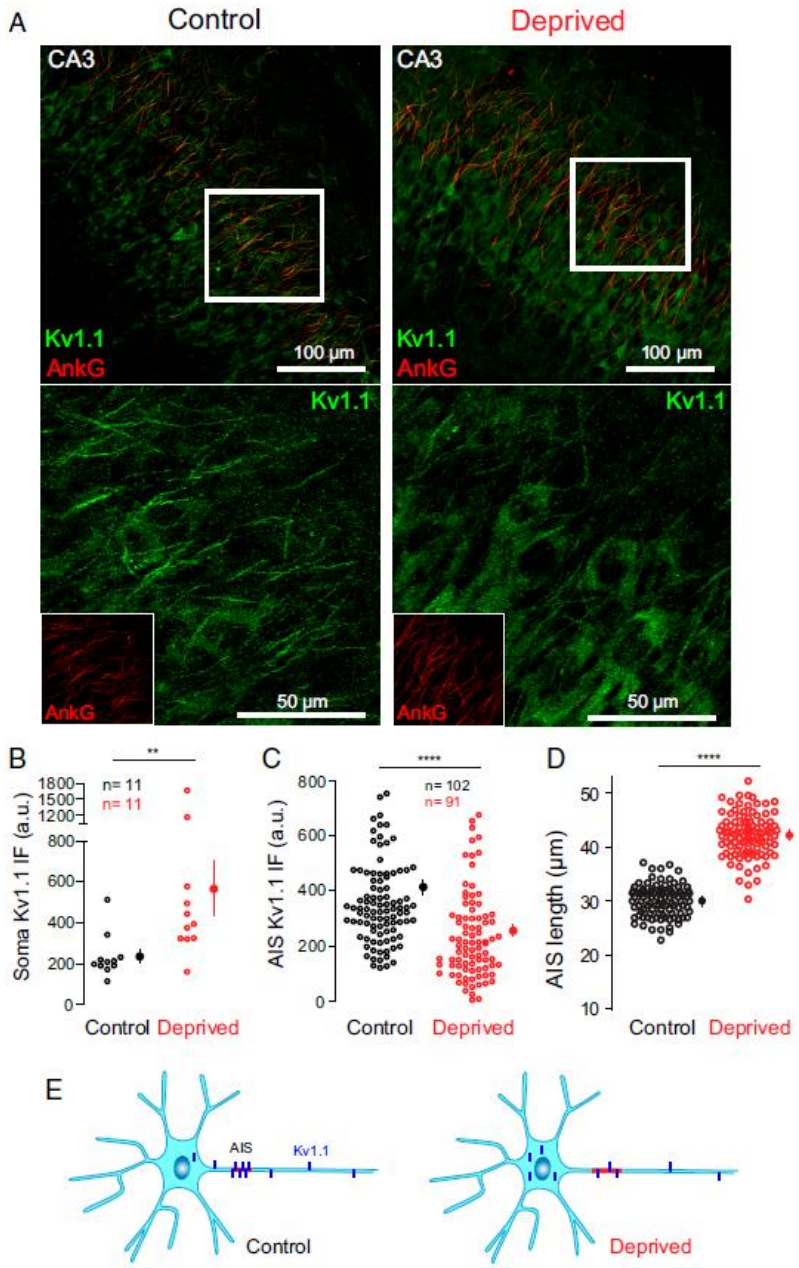

Fig. 2. Decrease in axonal Kv1.1 expression in activity-deprived cultures. (A) Hippocampal CA3 region of control and deprived hippocampal slice cultures stained with Kv1.1 (green) and Ankyrin G (red) antibodies (Upper) analyzed on stacks of 25 confocal sections of 1 µm. Lower shows an amplified image of Kv1.1 staining in the region indicated in Upper panels (box). Ankyrin G staining of this region is included in their respective Lower panels. Note the decreased Kv1.1 expression at the AIS accompanied by an increase in neuronal somas in deprived cultures. (B) Kv1.1 integrated fluorescence intensity in neuronal somas of each slice (a.u., arbitrary units); **P < 0.01. (C) Kv1.1 integrated fluorescence intensity in AISs (a.u.); ****P < 0.0001. (D) AIS length in control and deprived slices; ****P < 0.0001. (E) Summary scheme of the Kv1.1 channel reorganization in control and deprived cultures.

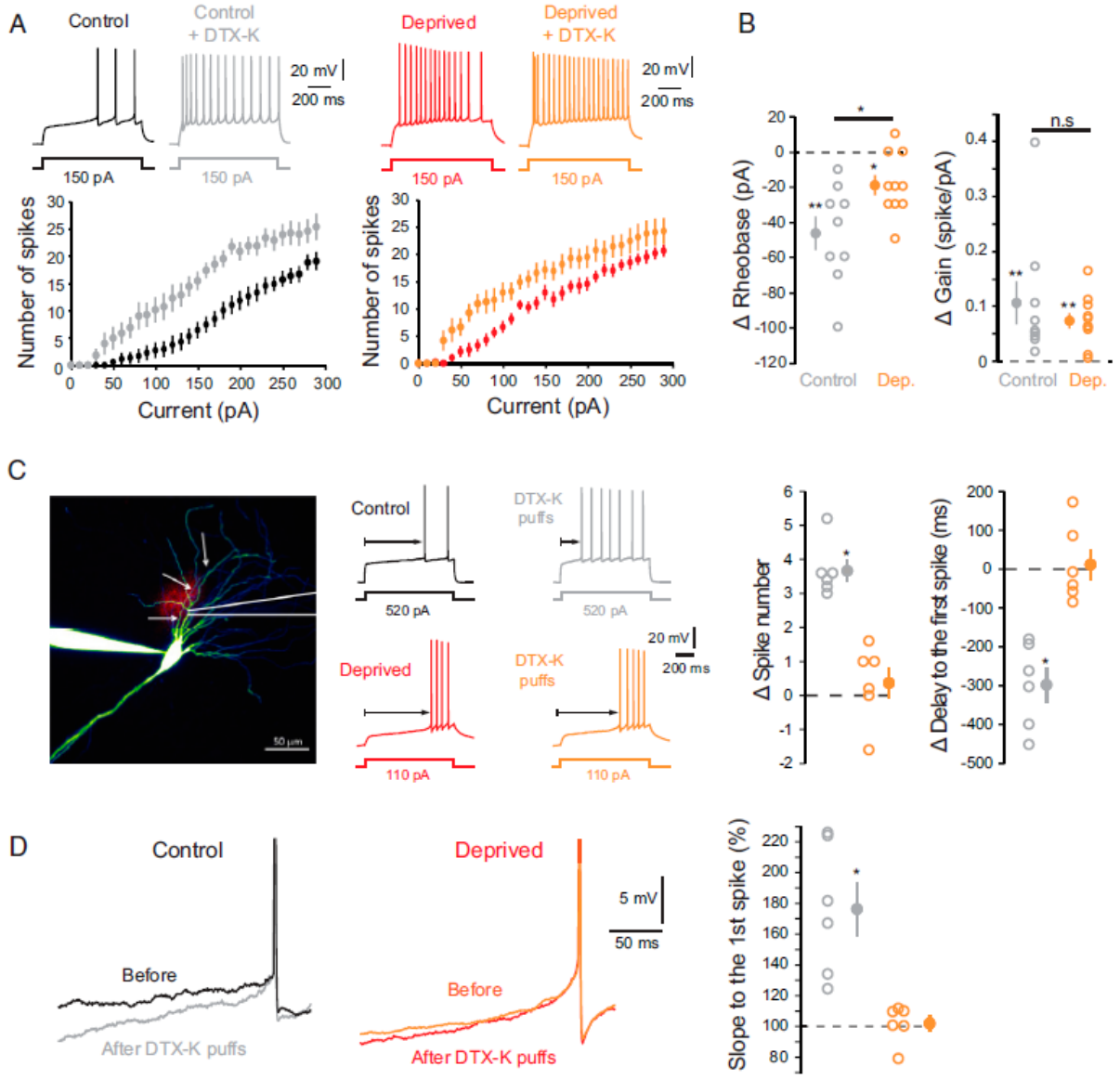

Fig. 3. Blockade of axonal Kv1.1 channels increases excitability in activity-deprived cultures. (A) Increase in intrinsic excitability in control and deprived cultures following DTX-K bath application. Top, Example current-clamp traces recorded in CA3 pyramidal neurons in control cultures (black: before DTX-K application; gray: after DTX-K application, n = 9) and in deprived cultures (red: before DTX-K application; orange: after DTX-K application, n = 10). Bottom, Average data across groups. (B) Left, Effect of DTX-K bath application on rheobase in control cultures (gray) and deprived cultures (orange). Note that the rheobase is reduced both in control cultures (Wilcoxon test: $P < 0.01$ [**]) and in deprived cultures (Wilcoxon test: $P < 0.05$ [*]) but the reduction is stronger in control cultures (Mann–Whitney U test: $P < 0.05$ [*]). Right, Effect of DTX-K bath application on input/output curve gain in control cultures (gray) and deprived cultures (orange). Note that the gain is increased both in control cultures (Wilcoxon test: $P < 0.01$ [**]) and in deprived cultures (Wilcoxon test: $P < 0.01$ [**]) and that this increase is similar in both conditions (Mann–Whitney U test: $P > 0.1$ [n.s.]). (C) Left, Example of a neuron filled with Alexa 488while a pipette is puffing DTX-K onto its axon (red spot). The arrows indicate the axon. Middle, Example current-clamp traces recorded in CA3 pyramidal neurons in control cultures (black: before DTX-K puffs; gray: after DTX-K puffs) and in deprived cultures (red: before DTX-K puffs; orange: after DTX-K puffs). Right, Plots for DTX-K axonal puff effects in control (gray, n = 6) and deprived cultures (orange, n = 6). Note that DTX-K puffs increase the number of APs evoked in control cultures but not in deprived cultures. Similarly, DTX-K puffs decrease the delay of the first AP evoked in control but not in deprived cultures; *$P < 0.05$. (D) Left, Example of the voltage depolarization slope before the first spike in control cultures (black: before DTX-K puffs; gray: after DTX-K puffs) and in deprived cultures (red: before DTX-K puffs; orange: after DTX-K puffs). Right, Plots for DTX-K axonal puff effects in control (gray, n= 6) and deprived cultures (orange, n = 6). Note that DTX-K puffs increase the voltage depolarization slope before the first spike in control cultures but not in deprived cultures; *$P < 0.05$.

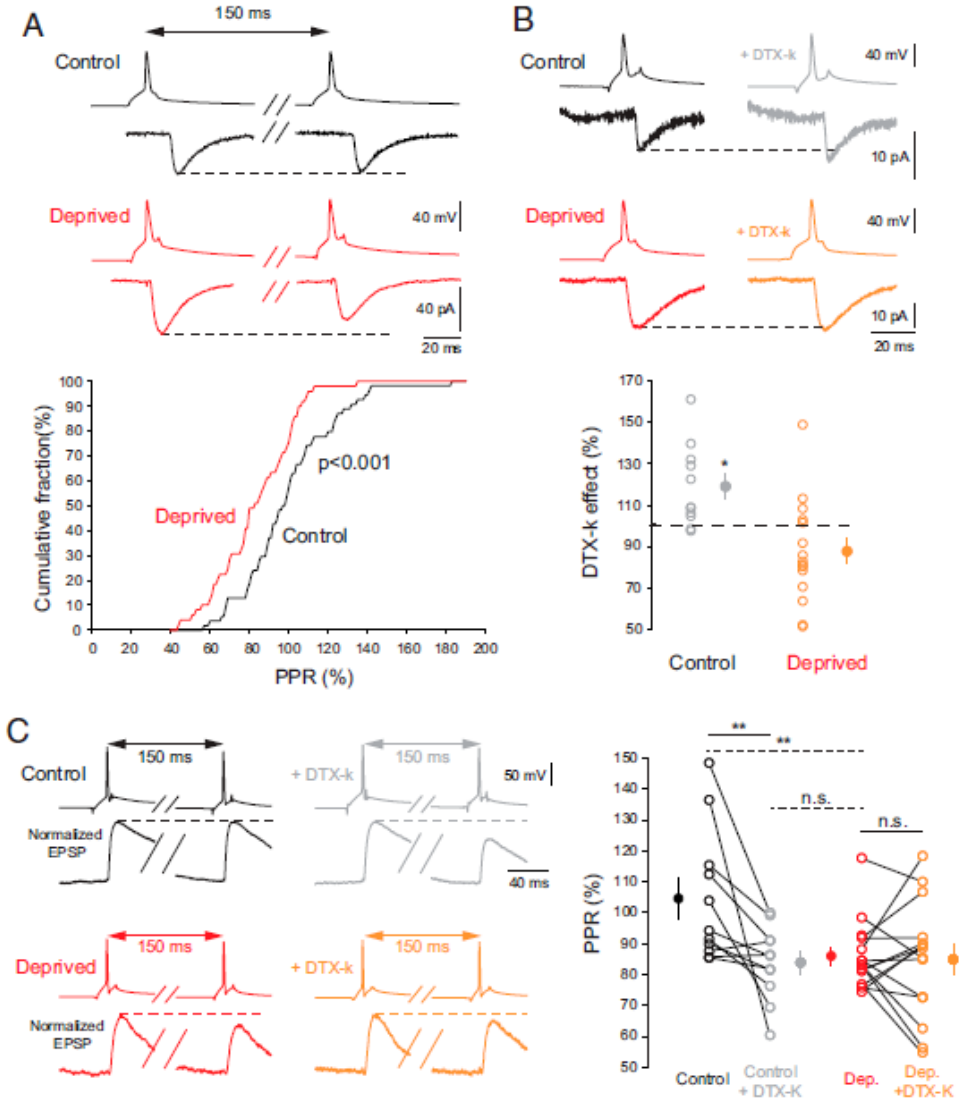

Fig. 4. Down-regulation of Kv1.1 channels increases glutamate release probability and synaptic strength in activity-deprived cultures. (A) Reduced PPR in deprived cultures (red) compared to control cultures (black). Top, Examples of CA3–CA3 synaptic responses in control and deprived cultures (average of 30 traces). Bottom, Cumulative histogram of PPR in control (black) and deprived (red) cultures. Note the leftward shift for deprived cultures showing a global decrease in PPR. (B) Kv1.1 channel blockade increases CA3–CA3 synaptic strength in control but not in deprived cultures. Top, Examples of Kv1.1 blockade effect on synaptic transmission in control cultures (black: before DTX-K application; gray: after DTX-K application) and deprived cultures (red: before DTX-K application; orange: after DTX-K application). Note the increase in synaptic transmission by DTX-K application in control but not in deprived cultures. Bottom, Plots for DTX-K effects on synaptic strength in control cultures (gray) and deprived cultures (orange); *P < 0.05. (C) Kv1.1 blockade increases release probability at CA3–CA3 synapses in control but not in deprived cultures. Left, Examples of Kv1.1 blockade effect on PPR in control cultures (black: before DTX-K application; gray: after DTX-K application) and deprived cultures (red: before DTX-K application; orange: after DTX-K application). Note the decrease in PPR by DTX-K application in control but not in deprived cultures. Right, Plots for DTX-K effects on PPR in control and deprived cultures (black: control, gray: control + DTX-K, red: deprived, orange: deprived + DTX-K). Note that the PPR is reduced in control cultures (control vs. control + DTX-K; Wilcoxon test: P < 0.01 [**]) but not in deprived cultures (deprived vs. deprived + DTX-K; Wilcoxon test: P > 0.1 [n.s.]). Importantly, the PPR is larger in control compared to deprived (Mann–Whitney U test: P < 0.01 [**]) but is similar between control + DTX-K and deprived (Mann–Whitney U test: P > 0.1 [n.s.]). Wilcoxon tests are represented by continuous lines and Mann Whitney U tests by dashed lines. Bonferroni correction for multiple comparison has been applied to the Mann–Whitney U tests.

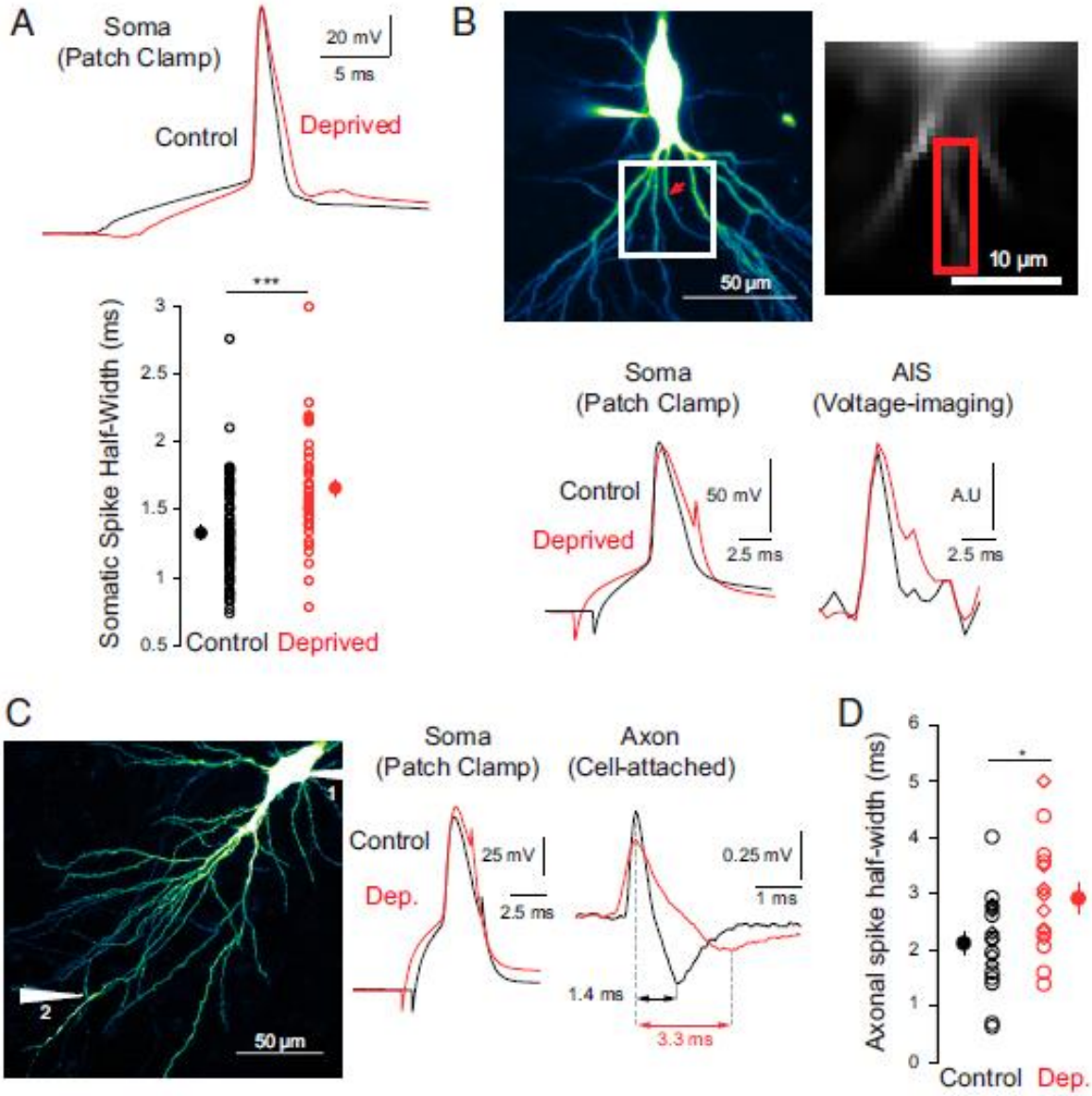

Fig. 5. Somatic and axonal action potentials are broader in activity-deprived cultures. (A) Somatic spike is broader in deprived cultures (red) compared to control cultures (black). Top, Examples of somatic spikes in control and deprived cultures. Bottom, Statistics of somatic spike half-width in control and deprived cultures; ***P < 0.001. (B) Top, Example of a CA3 neuron filled with Alexa 488 and JPW3028. Left image, Morphology of the neuron obtained following excitation of Alexa 488 (red arrow: axon). Right image, Fluorescence image obtained following excitation of JPW3028 (red rectangle: region of interest used to measure voltage-imaging signal). Bottom, Example of spikes recorded in the soma with electrophysiology (Left) and in the AIS with voltage imaging (Right) (control: black; deprived: red). Note that the axonal spike is broader in deprived cultures. (C) Left, Example of a CA3 neuron filled with Alexa 488. The axon collateral (white arrow number 2) is identified and recorded in cell-attached configuration. Right, Examples of spikes recorded in the soma in whole-cell mode and in the axon in cell-attached mode (control: black; deprived: red). Note that the peak-to-peak duration of the axonal signal is larger in deprived cultures. (D) Plot of axonal spike half-width in control and deprived cultures (open rhombi: individual voltage-imaging data points; open circles: individual cell-attached data points; closed circles: means; *P < 0.05).

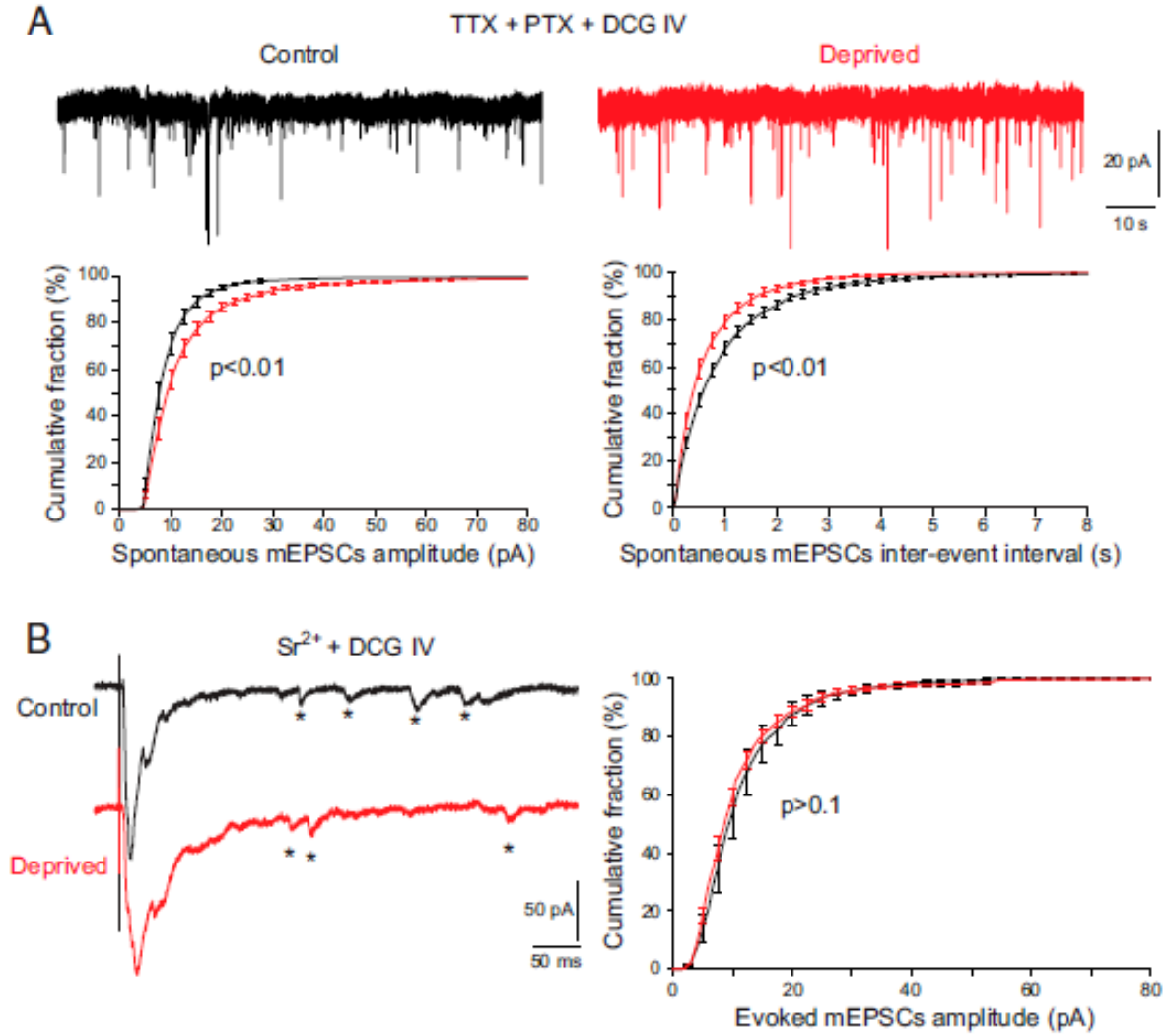

Fig. 6. Increase in spontaneous but not evoked mEPSC amplitude in activity-deprived cultures. (A) Spontaneous mEPSCs display increased amplitude and frequency in deprived cultures. Top, Examples of 1-min recordings of spontaneous mEPSCs (recorded in the presence of TTX, PTX, and DCG IV) in control (black) and deprived (red) cultures. Bottom Left, Cumulative histogram of spontaneous mEPSC amplitude in control (black) and deprived (red) cultures. Note the rightward shift for deprived cultures showing an increase in amplitude. Bottom Right, Cumulative histogram of spontaneous mEPSC interevent interval in control (black) and deprived (red) cultures. Note the leftward shift for deprived cultures showing an increase in frequency. (B) Evoked mEPSCs show no difference in amplitude in control and deprived cultures. Left, Examples of evoked mEPSCs (*, recorded 500 ms following extracellular stimulation in the presence of Sr2+ and DCG IV) in control (black) and deprived (red) cultures. Right, Cumulative histogram of evoked mEPSC amplitudes in control (black) and deprived (red) cultures.

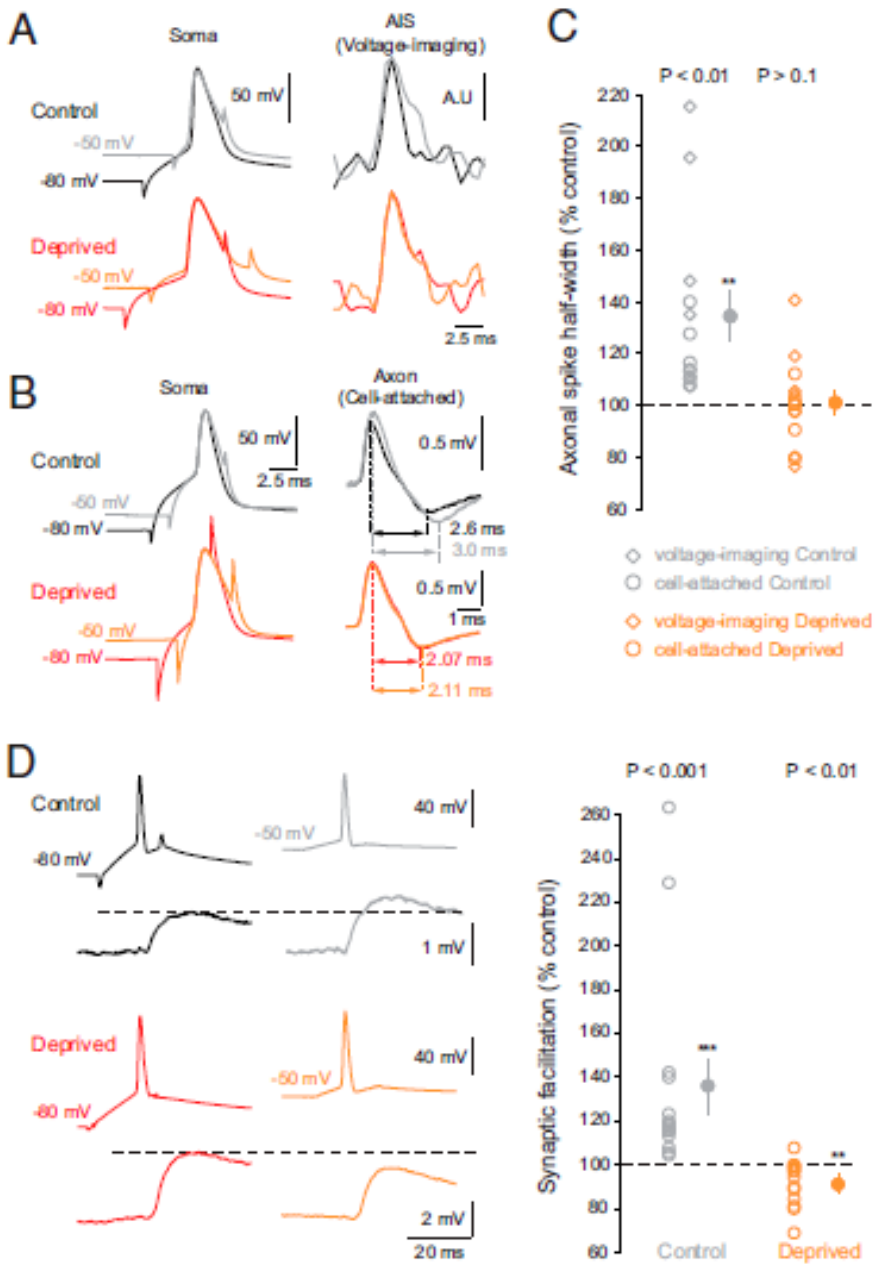

Fig. 7. Loss of depolarization-induced axonal spike broadening and synaptic facilitation in activity-deprived cultures. (A) Examples of spikes recorded in the soma with electrophysiology and in the AIS with voltage imaging. Note the broadening of the axonal spike at depolarized membrane potential in control cultures (black: hyperpolarized membrane potential; gray: depolarized membrane potential) but not deprived cultures (red: hyperpolarized membrane potential; orange: depolarized membrane potential). (B) Examples of spikes recorded in the soma in whole-cell mode (Left) and in the axon in cell-attached mode (Right). Note the increase in peak-to peak duration of the axonal spike at depolarized membrane potential in control cultures (black: hyperpolarized membrane potential; gray: depolarized membrane potential) but not deprived cultures (red: hyperpolarized membrane potential; orange: depolarized membrane potential). (C) Plot for subthreshold depolarization effect on axonal spike width in control cultures (gray) and deprived cultures (orange) (open rhombi: individual voltage imaging data points, open circles: individual cell-attached data points, closed circles: means); **P < 0.01. (D) Reversion of d-ADF in deprived cultures. Left Top, Example of CA3–CA3 connection showing presynaptic depolarization-induced facilitation in a control culture (black: hyperpolarized presynaptic membrane potential; gray: depolarized presynaptic membrane potential). Left Bottom, CA3–CA3 connection shows a presynaptic depolarization-induced depression in a deprived culture (red: hyperpolarized presynaptic membrane potential; orange: depolarized presynaptic membrane potential). Right, Plot for presynaptic depolarization effects on synaptic strength in control cultures (gray) and deprived cultures (orange); **P < 0.01; ***P < 0.001.